Measurement of γ rays from giant resonances excited by the ^{12}C(p, p') reaction at 392 MeV and 0°

M. S. Reen,[1,*] I. Ou,[1] T. Sudo,[1] D. Fukuda,[1] T. Mori,[1] A. Ali,[1] Y. Koshio,[1] M. Sakuda,[1,†] A. Tamii,[2,‡] N. Aoi,[2] M. Yosoi,[2] E. Ideguchi,[2] T. Suzuki,[2] T. Yamamoto,[2] C. Iwamoto,[3] T. Kawabata,[4] S. Adachi,[5] M. Tsumura,[5] M. Murata,[5] T. Furuno,[5] H. Akimune,[6] T. Yano,[7] T. Suzuki,[8] and R. Dhir[9]

[1]*Department of Physics, Okayama University, 700-8530 Okayama, Japan*
[2]*Research Center for Nuclear Physics (RCNP), Osaka University, 567-0047 Osaka, Japan*
[3]*Center for Nuclear Study, University Of Tokyo (CNS) RIKEN campus, 351-0198 Saitama, Japan*
[4]*Department of Physics, Osaka University, 567-0043 Osaka, Japan*
[5]*Department of Physics, Kyoto University, 606-8502 Kyoto, Japan*
[6]*Department of Physics, Konan University, 658-8501 Hyogo, Japan*
[7]*Department of Physics, Kobe University, 657-8501 Hyogo, Japan*
[8]*Department of Physics, Nihon University, 156-8550 Tokyo, Japan*
[9]*Department of Physics and Nanotechnology, SRM Institute of Science and Technology, 603203 Kattankulathur, India*

(Received 1 February 2019; revised manuscript received 1 July 2019; published 16 August 2019)

We measured both the differential cross section ($\sigma_{p,p'} = d^2\sigma/d\Omega dE_x$) and the γ-ray emission probability [$R_\gamma(E_x) = \sigma_{p,p'\gamma}/\sigma_{p,p'}$] from the giant resonances excited by ^{12}C(p, p') reaction at 392 MeV and 0°, using a magnetic spectrometer and an array of NaI(Tl) counters. The absolute value of $R_\gamma(E_x)$ was calibrated by using the well-known γ-ray emission probability from ^{12}C*(15.11 MeV, 1^+, $T = 1$) and ^{16}O*(6.9 MeV, 2^+, $T = 0$) states within 5% uncertainty. We found that $R_\gamma(E_x)$ starts from zero at $E_x = 16$ MeV, increases to a maximum of $53.3 \pm 0.4 \pm 3.9\%$ at $E_x = 27$ MeV, and then decreases. We also compared the measured values of $R_\gamma(E_x)$ with statistical model calculation based on the Hauser-Feshbach formalism in the energy region $E_x = 16$–32 MeV and discussed the features of γ-ray emission probability quantitatively.

DOI: 10.1103/PhysRevC.100.024615

I. INTRODUCTION

Carbon is the fourth most abundant element by mass in the solar system [1] after hydrogen, helium, and oxygen, and ^{12}C is its most abundant (98.9%) isotope. Thus, it has been used as a target material in the form of organic liquid scintillators in many large-scale neutrino experiments designed to detect low-energy neutrinos ($E_\nu < 100$ MeV) [2–6]. These detectors must be massive to compensate for the extremely small neutrino cross section ($\approx 10^{-42}$ cm^2). One of the most interesting applications is the detection of neutrinos from supernova explosion in our Galaxy [7,8]. The main reaction for neutrino detection is the charged-current (CC) antineutrino reaction with a proton ($\bar{\nu}_e + p \rightarrow e^+ + n$), also known as the inverse β-decay reaction (IBD). Of special interest is the neutral-current (NC) neutrino or antineutrino inelastic scattering with ^{12}C, followed by the emission of γ rays that can be observed with the detector [9]. This process is of a special interest because the cross section is significant enough to be detected and is independent of neutrino oscillations.

The first observation of ^{12}C(ν, ν')^{12}C*(15.11 MeV, 1^+, $T = 1$) reaction with 15.11-MeV γ ray came from the KARMEN experiment [4,5] with a neutrino beam. The observation was based on the detection of the electromagnetic decay of ^{12}C excited by neutral current interactions. The γ-ray emission probability (Γ_γ/Γ) of excited states of ^{12}C below the proton separation energy ($S_p = 16.0$ MeV) has been well measured [10]. However, the giant resonances appear above the separation energy and they decay mainly hadronically via particle emission (p, n, d, and α) to the daughter nuclei. Although they decay mainly to the ground state of the daughter nuclei (^{11}B, ^{11}C, etc.), some of these decays are to excited states. If these excited states are below the particle emission threshold in ^{11}B ($S_{p'} = 11.2$ MeV) or ^{11}C ($S_{p'} = 8.7$ MeV), they decay by γ-ray emissions. Kolbe *et al.* and Langanke *et al.* [11,12] proposed the above decay mechanism of giant resonances and estimated the NC neutrino and antineutrino reaction cross sections for ^{12}C and ^{16}O.

They stressed the importance of measuring NC events, since they are more sensitive to ν_μ and ν_τ neutrinos than to ν_e neutrinos.[1] However, there are no experimental measurements of γ rays from the giant resonances of ^{12}C.

In this paper, we report the first measurement of γ rays from the excited states of ^{12}C, including giant resonances in the energy region $E_x = 16$–32 MeV.

*mandeepsingh@okayama-u.ac.jp
†sakuda-m@okayama-u.ac.jp
‡tamii@rcnp.osaka-u.ac.jp

[1]This statement is based on the past predictions for the average neutrino energies [7,13]. The more recent calculations on neutrino spectra from supernova explosion suggest that the average neutrino energies are not very different between neutrino flavors [14].

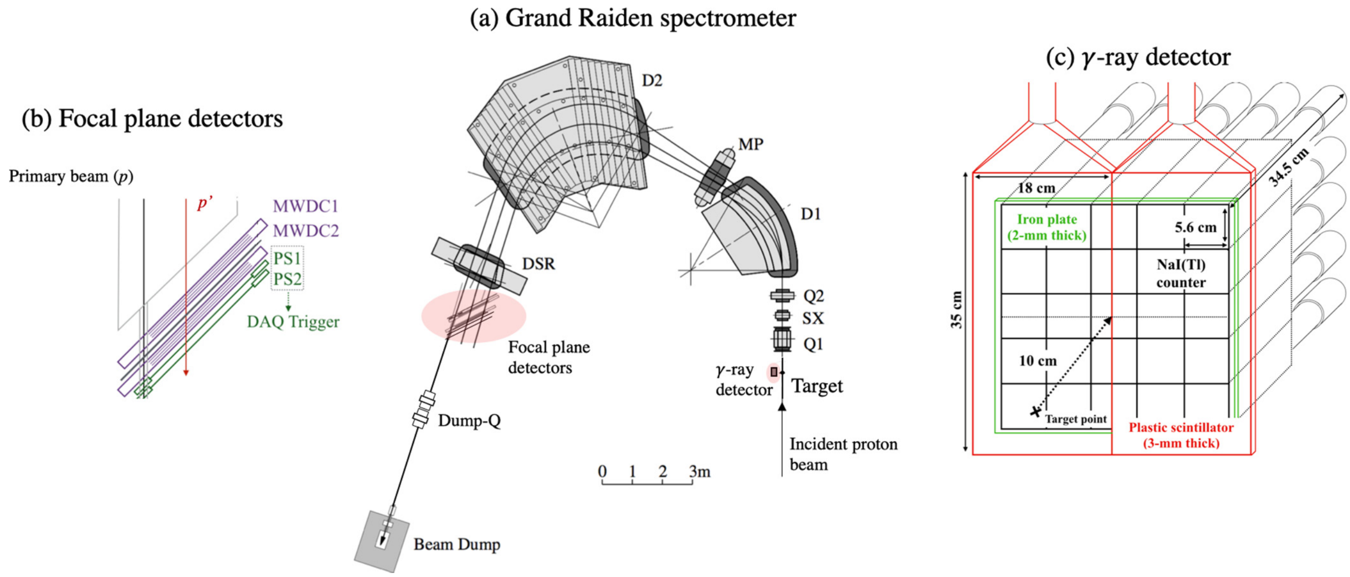

FIG. 1. (a) Grand Raiden spectrometer in the experimental setup at 0°, (b) focal plane detectors, and (c) γ-ray detector.

II. EXPERIMENT

The experiment (E398) to measure the γ rays emitted from giant resonances in ^{12}C was carried out at the Research Center for Nuclear Physics (RCNP), Osaka University. An unpolarized proton beam at 392 MeV bombarded a natural carbon ($^{\mathrm{nat}}$C) target with a beam bunch interval of 59 ns. The scattered protons were measured around 0° and were analyzed by the high-resolution magnetic spectrometer Grand Raiden (GR) [15]. The layout of (a) Grand Raiden (GR) spectrometer, (b) focal plane detectors, and (c) γ-ray detector is shown in Fig. 1.

A. Grand Raiden magnetic spectrometer

Two multiwire drift chambers (MWDCs) were placed at the focal plane of the GR system followed by two plastic scintillators (PS1 and PS2). Each of PS1 and PS2 was coupled with two photomultiplier tubes (PMT) from each side. A fast trigger (PS trigger) was generated by the coincidence of the discriminator signals of PS1 and PS2 for the data-acquisition (DAQ) system. Signals from the MWDCs were preamplified and discriminated by a LeCroy 2735DC board and the timing information of the wires was digitized by a LeCroy 3377 time-to-digital converter (TDC). The details of the DAQ system were described elsewhere [16] and only the components necessary for the present paper are described here. The MWDCs measure a charged-particle track at the focal plane of the GR spectrometer and were used to measure the excitation energy of the target nucleus ($E_x = E_p - E_{p'}$) and the scattering angle of protons (θ_p) at the target position. The spectrometer covered the scattering angle range of $0° < \theta_{\mathrm{p}} < 3.5°$. The beam current was monitored by a Faraday cup located at the beam dump and the typical beam intensity was 0.5–1.5 nA. An energy resolution of 120 keV (full width at half maximum) was achieved at $E_x = 15.1$ MeV. Details of the GR spectrometer have been described elsewhere [17,18].

B. γ-ray detector

A γ-ray detector was made from an array of 5×5 NaI(Tl) counters. One NaI(Tl) counter was made up of a 5.1 cm $\times$ 5.1 cm $\times$ 15.2 cm crystal and a photomultiplier (Hamamatsu R980) whose photo cathode (3.8 cm in diameter) was attached to one end of the crystal. The crystal was contained in an airtight 1-mm-thick aluminum case and a thin white reflective sheet was inserted between the crystal and the aluminum case. Thus, one NaI(Tl) counter has a total size of 5.6 cm $\times$ 5.6 cm $\times$ 34.5 cm. Each photomultiplier was covered by a μ metal. The γ-ray detector array was placed at $\theta = 90°$ with respect to the beam direction and at a distance of 10 cm from the target. The front face and sides of the detector were covered by a 2-mm-thick iron plate to suppress low-energy beam-induced and ambient γ rays less than 200 keV. Two 3-mm-thick plastic scintillators (veto counters) were attached in front of the iron plate and the NaI(Tl) counters to separate the background caused by charged particles directly entering the γ-ray detector. The scintillation light was measured from one end of the scintillator by a photomultiplier (Hamamatsu H6410) through an acrylic light guide.

For each PS trigger, both the ADC (charge information) and TDC (time information) of each PS counter were recorded. The GAM (GAMma-ray detector) signal is defined as the sum of discriminator signals of all NaI(Tl) counters. A GAM trigger was generated by taking the coincidence of the PS trigger and the GAM signal, and was used for the data acquisition of ADC and TDC of NaI(Tl) counters and veto counters. Those signals were digitized and recorded by LeCroy FERA and FERET systems.

While the initial energy calibration for all NaI(Tl) counters was performed by using a ^{60}Co source before the experiment, the energy response of the NaI(Tl) counters decreased gradually under the exposure of beam due to irradiation by beam-induced particles. Therefore, we calibrated the energy response of each NaI(Tl) counter for each run (typically

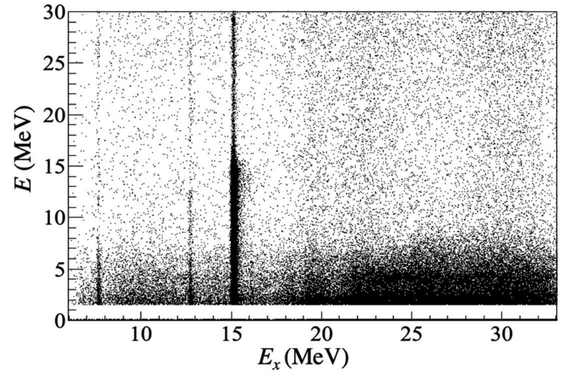

FIG. 2. Two-dimensional histogram with E (γ-ray energy measured by the detector) at y axis and E_x at x axis with each point showing a coincidence event. Accidental background has not been subtracted.

2 h) by using the following *in situ* γ rays, ^{12}C(15.11 MeV, 1^+), ^{11}B(2.12 MeV, $1/2^-$), and 1.37 MeV from ^{24}Mg*. The 1.37 MeV γ ray was induced by secondary interactions with the aluminum of the chamber surrounding the target. The mean energy of 1.37 MeV was determined by the nearby germanium counter. During the *in situ* calibration, we found that 15 downstream counters had poor energy resolution, so we used only the other ten upstream counters. The energy resolution $\sigma(E)/E$ of each of the ten upstream counters was 5% at 2 MeV and 3% at 15 MeV. The experiment was conducted with three beam intensities, 0.5, 1.0, and 1.5 nA, but the gain variation was the least for the 0.5-nA dataset. Therefore, that dataset was used for the γ-ray analysis.

C. Scattered proton and γ-ray coincidence measurement

The main feature of this experiment is to measure both the excitation energy E_x by the GR spectrometer and the γ-ray energy (E) by the NaI(Tl) counters. We define the γ-ray energy (E) as the sum of the pulse height measured in the upstream 10 NaI(Tl) counters. Thus, we study both the cross section ($\sigma_{p,p'} = d^2\sigma/d\Omega dE_x$) and the γ-ray emission probability [$R_\gamma(E_x) = \sigma_{p,p'\gamma}/\sigma_{p,p'}$] from the giant resonances. Figure 2 presents the spectra of the excitation energy (E_x) and the measured γ-ray energy (E) for the coincidence events between the PS trigger and the GAM trigger.

By taking a typical γ ray, 15.11 MeV, we explain in the following how we measured the γ-ray energy (E) and estimated the accidental background by using both ADC and TDC information for each E_x interval. The time difference between the GAM trigger and the PS trigger is plotted in Fig. 3 for γ rays from ^{12}C(15.11 MeV, 1^+, $T = 1$). Events in the prominent first peak (red) were selected as coincidence events between the two triggers, whereas those in the other peaks were selected as accidental background. Pulse intervals of 59 ns correspond to the bunch structure of the beam. Thus, we obtained the energy deposit E for the signal (red line) and the background (blue line) for $E_x = 15.11$ MeV in Fig. 3(b). The details of the analysis will follow in Secs. III and IV.

III. ANALYSIS OF SCATTERED PROTONS

A. (p, p') differential cross section

The double differential cross section is given as

$$\sigma_{p,p'} \equiv \frac{d^2\sigma}{d\Omega dE_x} = J\frac{N_{E_x}}{\Delta E_x}\frac{1}{\Omega}\frac{1}{L\eta}\frac{e}{Q}\frac{A}{N_A\rho}, \tag{1}$$

where J is the Jacobian for the transformation from laboratory frame to c.m. (center of mass) frame (0.81), η is the tracking and trigger efficiency (0.91), L is the DAQ live time, e is the elementary charge (C), Q is the total beam charge (C), and N_{E_x} are the number of excitation events in the energy range E_x and $E_x + \Delta E_x$ obtained after subtracting the background. The detailed procedure for background subtraction was provided in Ref. [18]. Furthermore, A is the atomic weight (g/mol), N_A is the Avogadro constant, and ρ is the areal density (36.3 mg/cm^2). The spectrometer acceptance was not symmetrical with respect to the horizontal and vertical directions (-9 mrad $\leqslant \theta_x \leqslant 0$ mrad, $|\theta_y| \leqslant 43$ mrad). The events were chosen within a solid angle (Ω) of 0.77 msr.

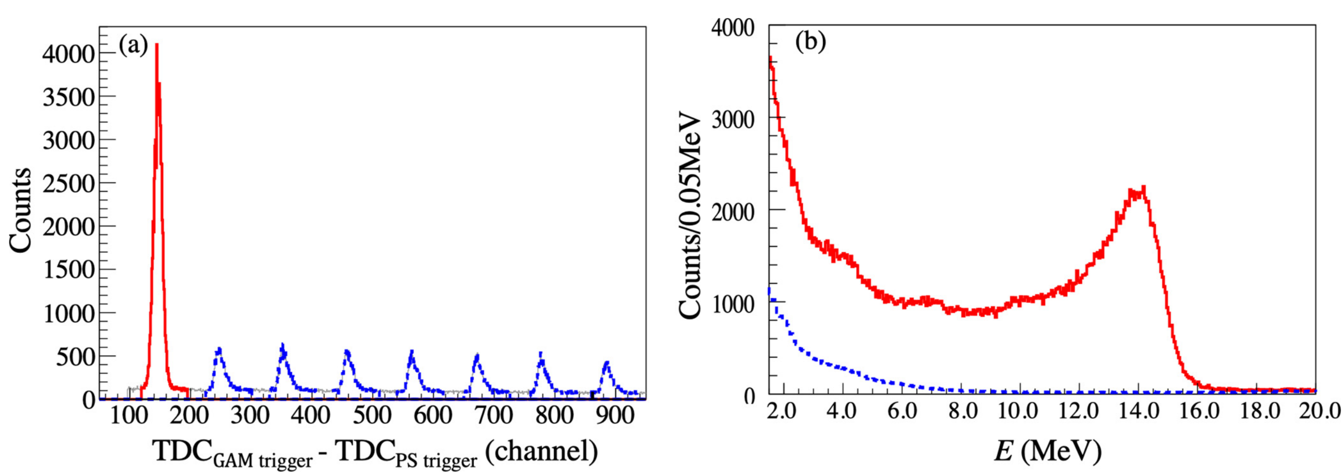

FIG. 3. (a) Time difference between GAM trigger and PS trigger. (b) γ-ray energy spectrum (red solid line) and background spectrum (blue dotted line) for the 15.11-MeV state (1^+, $T = 1$) of ^{12}C.

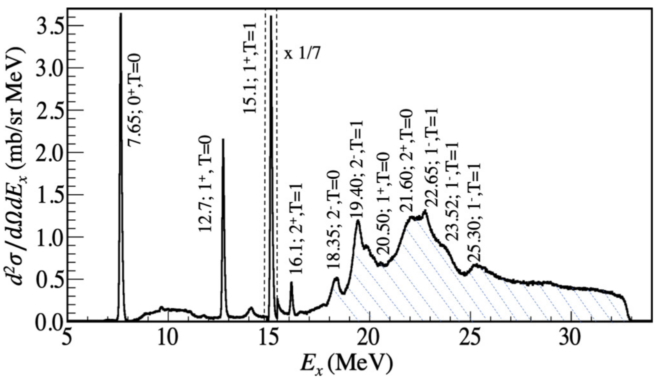

FIG. 4. Double differential cross section of the ^{12}C(p, p') reaction at $E_p = 392$ MeV and $\theta = 0^\circ$. The bin width is 0.02 MeV.

The measured cross section of ^{12}C(p, p') is shown in Fig. 4. The systematic uncertainties in the measurement are shown in Table I. Giant resonances are clearly seen in the spectrum. We list the excitation energies E_x, spin parities (J^π), and isospin (T) of the known resonances in Table II. We show the differential cross section for ^{12}C(15.11 MeV, 1^+, $T = 1$) and ^{16}O(11.5 MeV, 2^+, $T = 0$) in Fig. 5, demonstrating the consistency of our cross section with those of previous experiments performed with the same GR spectrometer at the same beam energy [21,22]. Our cross section measurements of ^{16}O(11.5 MeV, 2^+, $T = 0$) were performed during the same experiment with a cellulose ($C_6H_{10}O_5$) target. Both of our measured cross sections are consistent with those measured in previous experiments within the systematic uncertainty of 6%.

B. Decomposition of the cross section into spin-flip and non-spin-flip components

We now discuss the energy spectra shown in Fig. 4 in more detail. In a previous experiment [21], the polarization transfer (PT) observables were measured for ^{12}C(p, p') at the same beam energy and 0° in the GR spectrometer, in which the excitation strengths were decomposed into a spin-flip part ($\Delta S = 1$) and a non-spin-flip part ($\Delta S = 0$). Figure 6(a) shows the cross section $d^2\sigma/d\Omega dE_x$ (solid line), the same as that in Fig. 4, and the spin-flip cross section $\Sigma\ d^2\sigma/d\Omega dE_x$ (shaded region). The total spin transfer Σ is unity for spin-flip transitions ($\Delta S = 1$) and zero for non-spin-flip transitions ($\Delta S = 0$). We used the Σ values measured in the previous experiment [21], whereas the cross sections $d^2\sigma/d\Omega dE_x$ are our measurements. In the spin-flip cross section, excited states at $E_x = 18.35$, 19.4, 22–23, and 25 MeV were observed whereas the non-spin-flip cross section was dominated by broad resonances at $E_x = 22$–24 and 25–26 MeV.

TABLE I. Systematic uncertainties in the measurement of differential cross section.

Variable	Value
Tracking efficiency (η)	1%
Solid angle (Ω)	3%
Beam charge (Q)	3%
Target thickness (t)	2%
Background subtraction	3%
Total	6%

TABLE II. Resonance energy (E_m), resonance width (Γ_m), spin parity, and isospin obtained from Ref. [33], and σ_m obtained from fit. *1: Spin-parity and isospin were obtained from Refs. [21,30]. *2: E_m and Γ_m were obtained from Refs. [19,20].

E_m (MeV)	$J^\pi;T$	Γ_m (MeV)	σ_m (mb/sr MeV)
18.35*1	2^-;0	0.35 ± 0.05	0.35 ± 0.03
19.40	2^-;1	0.49 ± 0.03	0.90 ± 0.05
20.00	2^+	0.38 ± 0.10	0.39 ± 0.04
20.50*1	1^+;0	0.30 ± 0.05	0.15 ± 0.03
21.60	2^+;0	1.20 ± 0.15	0.18 ± 0.02
21.99	1^-;1	0.61 ± 0.11	0.19 ± 0.06
22.37	1^-;1	0.29 ± 0.04	0.01 ± 0.06
22.65	1^-;1	3.20 ± 0.20	0.84 ± 0.1
22.68*2	1^-;1	0.40 ± 0.04	0.19 ± 0.13
23.52	1^-;1	0.24 ± 0.02	0.06 ± 0.06
23.99	1^-;1	0.57 ± 0.12	0.04 ± 0.01
24.38	2^+;0	0.67 ± 0.06	0.00 ± 0.00
24.41		1.30 ± 0.30	0.00 ± 0.00
24.90		0.90 ± 0.20	0.00 ± 0.00
25.30	1^-;1	0.51 ± 0.10	0.19 ± 0.04
25.40	1^-	2.00 ± 0.20	0.00 ± 0.00
25.96	2^+	0.70 ± 0.20	0.14 ± 0.02
27.00	1^-;1	1.40 ± 0.20	0.11 ± 0.03
28.20	1^-;1	1.60 ± 0.20	0.06 ± 0.01
28.83		1.54 ± 0.09	0.09 ± 0.01
29.40	2^+;1	0.80 ± 0.20	0.02 ± 0.01
30.29	2^-;1	1.54 ± 0.09	0.04 ± 0.01
31.16		2.10 ± 0.15	0.07 ± 0.01
32.29		1.32 ± 0.23	0.01 ± 0.01
Quasifree Continuum			$\mu = 1.27 \pm 0.25$

C. Comparison of spin-flip cross sections with charge exchange reaction

We now compare our $\Sigma\ d^2\sigma/d\Omega dE_x$ [Fig. 6(a), shaded region] with the $T = 1$ charge-exchange ^{12}C(p, n)^{12}N spin-flip cross section measured at $E_p = 296$ MeV [23]. The latter (p, n) cross section was multiplied by a factor of 0.5 (the Clebsch-Gordan coefficients) in order to compare with (p, p') cross section. Moreover, the excitation energy was shifted for the case of the ^{12}C(p, n)^{12}N reaction by 15.1 MeV.

The $T = 1$ charge-exchange ^{12}C(p, n)^{12}N spin-flip cross section was also measured at $E_p = 135$ MeV by Anderson *et al.* [24] and both data agree within the given errors. Both observed resonances at $E_x = 19.4$ (2^-), 22–23 (2^-), and 25 (1^-) MeV. Our spin-flip cross sections (shaded region) agree with the $T = 1$ charge-exchange spin-flip cross sections, except for a small disagreement in the region $E_x = 18$–19.4 MeV. This obvious disagreement arises from the fact that

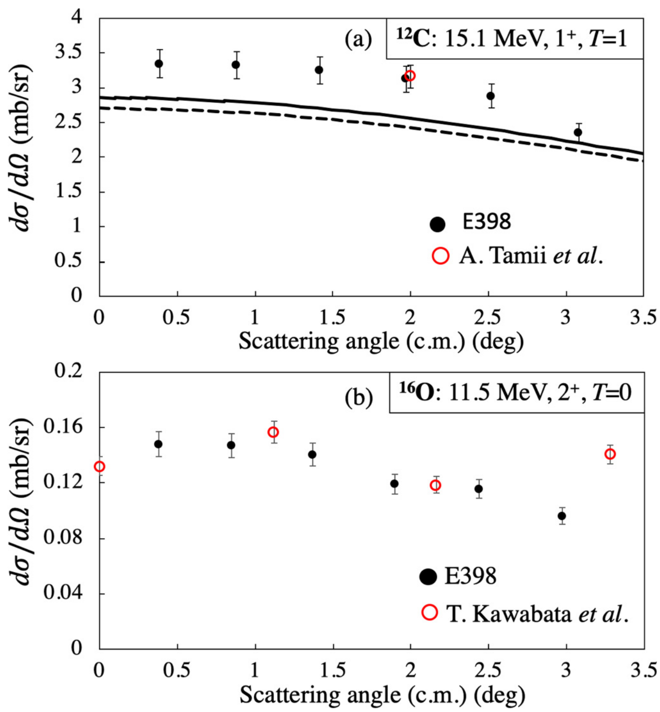

FIG. 5. (a) Differential cross section of the ^{12}C(p, p') reaction as a function of scattering angle (black circles) and comparison with previous experiment [21] (red open circles). Solid (SFO) and dashed (Cohen-Kurath) lines are the DWBA calculation results for the transitions to 15.1-MeV state (see text for details). (b) Differential cross section for ^{16}O(p, p') reaction as a function of scattering angle and comparison with previous experiment [22].

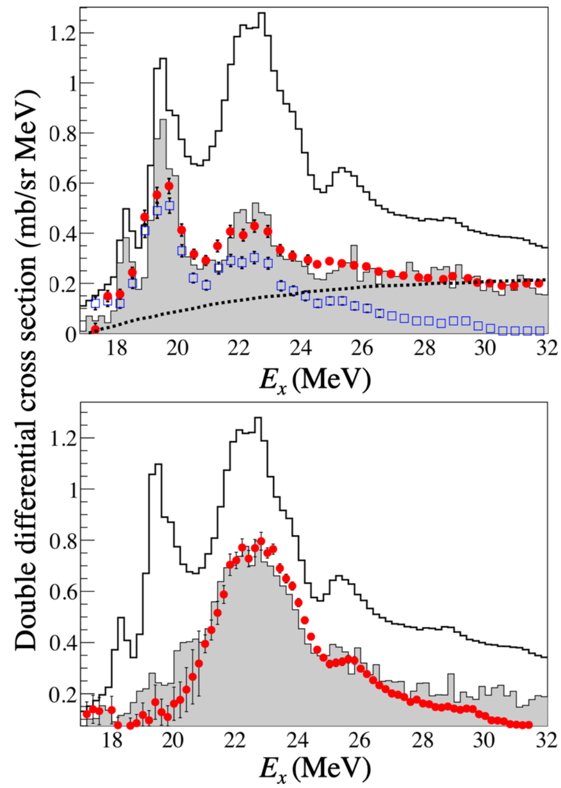

FIG. 6. (a) Spin-flip component $\Sigma\ d^2\sigma/d\Omega dE_x$ (shaded region) is compared with $d^2\sigma/d\Omega dE_x$ (solid line). The spin-flip cross section for ^{12}C$(p, n)^{12}$N reaction (blue open squares), the contribution of quasifree process (dotted line), and their sum (red circles) are obtained from Ref. [23]. (b) Non-spin-flip component $(1 - \Sigma)\ d^2\sigma/d\Omega dE_x$ (shaded region) is compared with $d^2\sigma/d\Omega dE_x$ (solid line). The calculation of Coulomb excitation (red circles) is also shown. The bin width is 0.2 MeV.

our data also include isoscalar resonance at $E_x = 18.35$ MeV, which is not observed in the charge exchange reaction. This comparison primarily indicates that the (p,p') spin-flip cross sections are mostly dominated by the $T = 1$ component, and the contribution of $T = 0$ is small.

Indeed, the authors of Refs. [25,26] performed the analysis of the effective interaction (V) based on the N-Nt matrix for the nucleon-nucleus scattering data over the energy range between 100 and 800 MeV. They found that the spin-isospin term $[V_{\sigma\tau}\ (T = 1)]$ in the effective interaction is much stronger than the spin term $[V_\sigma\ (T = 0)]$ and that it is independent of the beam energy.

D. Comparison of non-spin-flip cross sections with ^{12}C$(\gamma$,total) reaction

Figure 6(b) shows the cross section $d^2\sigma/d\Omega dE_x$ (solid line) and the non-spin-flip cross section $(1 - \Sigma)\ d^2\sigma/d\Omega dE_x$ (shaded region). It was suggested qualitatively by the ^{16}O(p, p') experiment at the same beam energy (392 MeV) and 0° [22] that the non-spin-flip cross section is dominated by isovector giant dipole resonance ($J^\pi = 1^-, T = 1$) which is related to the Coulomb excitations.

We examined this feature more quantitatively by using the latest calculation of the Coulomb excitation [15,27] in the forward (p, p') reaction, which is expressed in terms of the total photonuclear absorption cross section [28]. The Coulomb excitation cross section was calculated at 1° in Fig. 6(b), since the average proton scattering angle was about 1°. The calculation is shown in Fig. 6(b) and agrees fairly well with the non-spin-flip data, except for the low energy region $E_x =$ 18–21 MeV and the high energy region $E_x > 30$ MeV. In the low energy region our non-spin-flip data also include isoscalar resonance at $E_x = 20.5$ MeV which does not couple to the photoabsorption process and the data points are higher than the calculations. We also compared the calculation for Coulomb excitation with the non-spin-flip cross section for the ^{58}Ni(p, p') reaction measured at 0° in RCNP [29] and found a good agreement within 10%. Other small isoscalar contributions to the non-spin-flip cross section of ^{12}C for $E_x > 25$ MeV were reported in a ^{12}C(d, d') experiment [30] and a ^{12}C(α, α') experiment [31,32].

E. Decomposition of different excited states

It is clearly seen that the energy region $E_x =$ 16–32 MeV consists of many overlapping resonances with different spin parities and isospins. In order to unfold these resonances, we fit the cross section with known resonances [33] and a quasifree continuum. The resonances were assumed to have

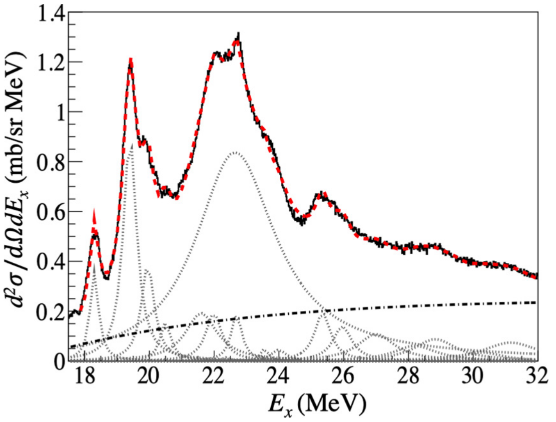

FIG. 7. Double differential cross section for the giant resonance region in ^{12}C fitted with various resonances (dotted lines) [33] and a quasifree continuum (dash-dotted line). The red dashed curve shows the overall fit obtained from the sum of all contributions.

Lorentzian distributions and the quasifree cross section was assumed to have a smooth functional form as described in Ref. [34] [also shown in Fig. 6(a)]. The overall fitting function was thus given as

$$f(E_x) = \sum_m \frac{\sigma_m}{1 + (E_x^2 - E_m^2)^2 / E_x^2 \Gamma_m^2} + \mu N \frac{1 - e^{[-(E_x - E_0)/T]}}{1 + [(E_x - E_{QF})/W_L]^2}, \quad (2)$$

where E_m and Γ_m are the peak energy and the resonance width, respectively, for the mth resonance. Their values were taken from Ref. [33] and kept fixed during the fitting. The values of N (0.2 mb/sr MeV), E_{QF} (27 MeV), W_L (55 MeV), E_0 (16 MeV), and T (6 MeV) were determined from fitting to the ^{12}C$(p, n)^{12}$N cross section [23] and were kept fixed during this fit. The parameters σ_m (peak cross section) and μ were determined to reproduce the data in the region of E_x = 18–32 MeV and are tabulated in Table II . The fit is shown in Fig. 7.

F. Angular distribution in comparison with DWBA calculations

We also present the differential cross section for the ^{12}C(p, p') reaction as a function of scattering angle in various E_x regions (Fig. 8). Some of the angular distributions were compared with DWBA calculations.

The DWBA calculations were performed with the program DWBA07 [35]. The single particle wave functions for the bound particles were of harmonic oscillator form. For the giant resonance region, the harmonic oscillator parameter b = 1.64 fm was adopted [36,37]. The distorted wave was derived by using an optical potential. The optical potential parameters were taken from Ref. [38], as determined from 398-MeV proton scattering from ^{12}C, and are listed in Table III. The effective NN interaction derived by Franey and Love [25] at E_p = 425 MeV was used. The transition densities were obtained from shell model calculations with SFO (Suzuki-Fujimoto-Otsuka) Hamiltonians [36,39] and are tabulated in Table IV.

In Fig. 6(a), it is clearly seen that the energy region E_x = 19–20 MeV is dominated by a spin-flip cross section, and the data shown in Fig. 8(a) show a clear angular dependence. The shape is well reproduced by the DWBA calculation results for the transitions to E_x = 19.4 MeV ($J^\pi = 2^-, T = 1$). For the energy region E_x = 22–24 MeV, which is dominated by Coulomb excitations, the calculation results for the transitions to E_x = 22.8 MeV ($J^\pi = 1^-, T = 1$) also reproduce the shape of angular distribution shown in Fig. 8(c). For $E_x > 24$ MeV, no clear angular dependence was observed.

We also tested DWBA for the cross section calculations of the 15.1-MeV state. The harmonic oscillator parameter was chosen [38,40] to match the prominent maxima of longitudi-

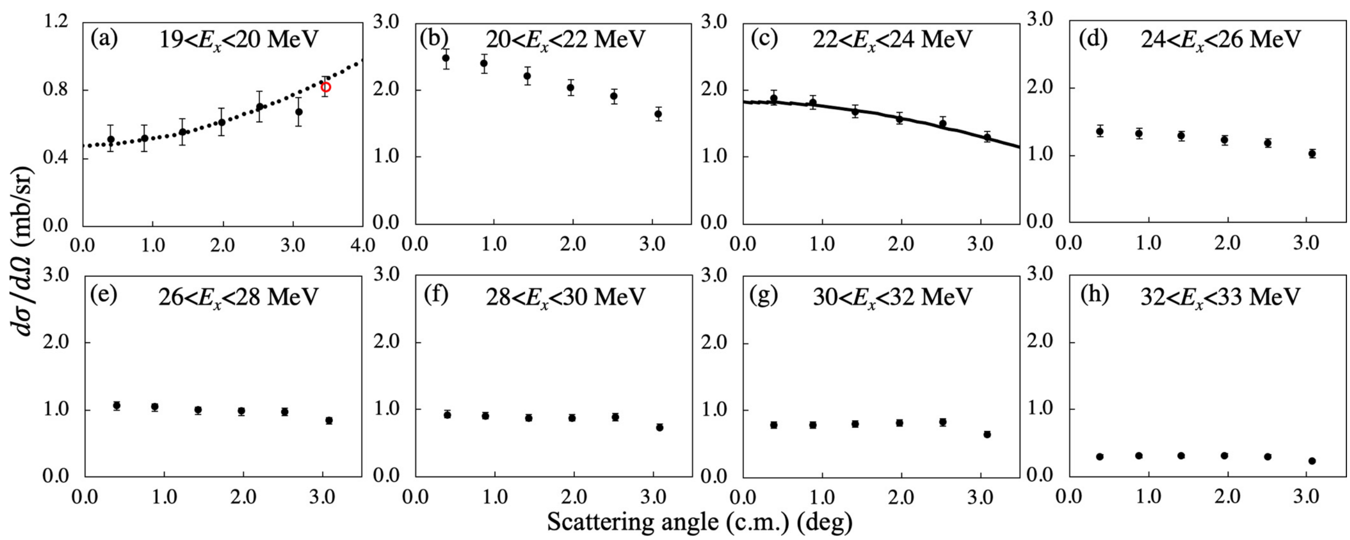

FIG. 8. Differential cross section as a function of scattering angle at various excitation energies in the giant resonance region of ^{12}C. Dotted and solid black lines show the result of DWBA calculations (see text). (a) A data point (red open circle) from another experiment [38] is also shown.

TABLE III. Optical model parameters used in DWBA calculations taken from Ref. [38].

E_p (MeV)	V (MeV)	r_0 (fm)	a_0 (fm)	W_v (MeV)	r_0' (fm)	a_0' (fm)	V_{LS} (MeV)	r_{LS} (fm)	a_{LS} (fm)	W_{LS} (MeV)	r_{LS}' (fm)	a_{LS}' (fm)	r_{0C}
398	−2.51	1.08	0.48	21.6	1.13	0.64	3.21	0.93	0.57	−2.79	1.00	0.53	1.05

nal and transverse form factors [$F_L(q)$ and $F_T(q)$] measured in a previous electron scattering experiment [37]. Two types of transition densities were used for the calculations of the 15.1-MeV state (Table IV), the transition densities obtained from shell model calculations with SFO Hamiltonians [36,39] and $1p$ shell transition densities from Cohen and Kurath [38,41]. The comparison between calculations for these two different transition densities is shown in Fig. 5(a), along with the measured cross section. The dashed line represents the calculated cross section with transition densities from SFO Hamiltonians, and the solid line was obtained with Cohen and Kurath transition densities and was scaled by a factor of 1.15 [38].

IV. ANALYSIS OF EMITTED γ RAYS

A. Definition and generation of response function $P(E_\gamma; E)$

The response functions of the γ-ray detector were generated by geant4 Monte Carlo simulations (MC) [42]. The response function $P(E_\gamma; E)$ is defined as the probability for a γ ray of energy E_γ irradiated uniformly upon the target position to be measured as energy E by the γ-ray detector, and

$$\int_{E_{\rm th}}^{E_{\rm max}} P(E_\gamma; E)dE = \eta(E_\gamma), \tag{3}$$

where $\eta(E_\gamma)$ is the detection efficiency for a γ ray of energy E_γ. For the present case, the threshold ($E_{\rm th}$) for the γ-ray detectors was chosen to be 1.5 MeV. The detector geometry and the effect of the materials between the target and detector were taken into account during the detector simulation. The accuracy of the response function was tested by comparison with the γ-ray spectra of 15.1 and 6.9 MeV measured during the experiment.

To generate the response function of a 15.1-MeV γ ray, cascade γ rays from the 15.1-MeV state [33], 10.66, 7.45, 4.8, 4.4, and 2.4 MeV, were also taken into account, along with their respective branching ratios. The response function was then normalized by the 15.1-MeV excitation counts measured by the spectrometer in the energy range of $E_x = 14.9$–15.4 MeV. Further, we determined the correction factor (0.88) for the response function to account for the dead time of the γ-ray detector by normalizing the data to reproduce the well-measured 15.1-MeV γ-ray emission probability ($\Gamma_\gamma/\Gamma = 0.96 \pm 0.04$). The response function for a 15.1-MeV γ ray is shown in Fig. 9(a) (red line) along with the γ-ray energy spectrum measured from the ^{12}C (15.1 MeV, 1^+) (black points) after subtracting the background spectrum. The procedure for measuring the γ-ray spectrum and background subtraction was described in Sec. II C and shown in Fig. 3. The photopeak and single- and double-escape peaks appear as one broad peak due to the resolution of the γ-ray detector. This correction factor (0.88) was used to scale the response function of all the other γ rays.

B. Validation of response function $P(E_\gamma; E)$

We show in Fig. 9(b) the γ-ray spectrum (after background subtraction), as measured from $E_x(^{16}\mathrm{O}) = 6.9$–7.3 MeV. Within this range, two states of ^{16}O, 6.9 and 7.1 MeV, were excited. These states decay to the ground state by emitting 6.9- and 7.1-MeV γ rays, respectively, with 100% emission probability. The response functions were generated for 6.9 and 7.1 MeV and weighted according to their contribution. A comparison with the response function normalized by excitation counts in the same E_x range is shown in Fig. 9(b). When the value of data/MC for 15.1 MeV was normalized to 1.0 with the correction factor (0.88), the same factor yields data/MC = 0.98 ± 0.02 for 6.9 MeV (including 7.1 MeV). The efficiency [$\eta(E_\gamma)$] was evaluated to be 2.3% for $E_\gamma = 2.0$ MeV and 5.9% for $E_\gamma = 15.1$ MeV.

For the lower γ-ray energy range, the consistency was checked with a ^{60}Co source that emits two simultaneous γ rays with energies of 1.13 and 1.33 MeV. The response function generated for ^{60}Co reproduced the data within an

TABLE IV. Transition matrix elements used in DWBA calculations. The superscript (a) denotes transition matrix elements from Cohen and Kurath [38] and (b) denotes matrix elements obtained from SFO Hamiltonian [36,39]. The amplitude for the component $l_i l_j$ represents an excitation from the l_j hole state to the l_i particle state. The subscripts on the single-particle orbitals represent the quantity $2j$. Here, the $2s_{1/2}$ orbital is designated as s_1.

E_x (MeV)	$J^\pi; T$	b (fm)	d_3p_1	d_3p_3	d_5p_3	s_1p_3	d_5p_1	p_1p_1	p_1p_3	p_3p_1	p_3p_3
15.1$^{(a)}$	$1^+; 1$	1.86						−0.0581	−0.6901	−0.3394	−0.0764
15.1$^{(b)}$	$1^+; 1$	1.86						0.0829	0.6701	0.2904	0.0841
19.4$^{(b)}$	$2^-; 1$	1.64		−0.0926	0.5415	0.3043	−0.3047				
22.8$^{(b)}$	$1^-; 1$	1.64	−0.1263	0.1472	−0.6874	−0.2108					

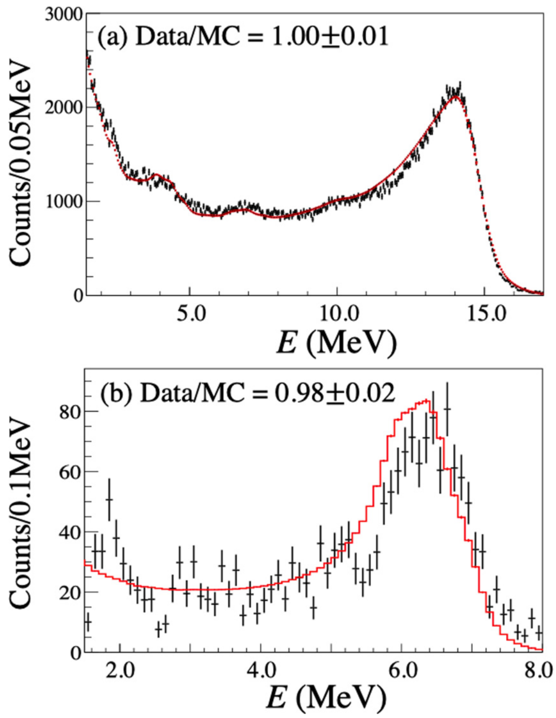

FIG. 9. Measured γ-ray spectrum (black data points) after background subtraction and response function (red line) for the (a) 15.11-MeV state ($J^\pi = 1^+$) of ^{12}C and (b) 6.9-MeV state ($J^\pi = 2^+$) of ^{16}O (see text for details).

uncertainty of 3%. The consistency between data and response function within the systematic uncertainty of 5% validates our measurement of γ-ray emission probability for the energy range from 1.1 to 15.1 MeV.

V. γ RAYS FROM THE GIANT RESONANCES

A. γ-ray energy spectra for each E_x bin

The γ-ray energy spectra from the giant resonances were measured for various E_x values with a 2-MeV energy step. Figure 10 (left) shows the measured γ-ray energy spectrum (black line) and background spectrum (red line). The decay scheme of excited ^{12}C is also shown.

As E_x reaches the proton separation energy ($S_p = 16.0$ MeV), the ^{12}C state decays hadronically to the ground state of ^{11}B by emitting a proton. No γ-ray emission is possible until E_x exceeds the threshold ($S_p + 2.1 = 18.1$ MeV) for proton decay to the first excited state of ^{11}B*(2.1 MeV). This feature was confirmed experimentally as no γ rays were observed from the region $E_x = 16$–18 MeV [shown in Fig. 10(a)]. The same feature can be seen in Fig. 10(b) where we observed only a 2.1-MeV γ ray, as the 2.1-MeV state of ^{11}B is the only energetically accessible state at $E_x = 18$–20 MeV. As E_x reaches 21 MeV, the ^{12}C state can decay to the second (4.4 MeV) and third (5.0 MeV) excited states of ^{11}B or to the first excited state of ^{11}C*(2.0 MeV), after neutron emission ($S_n + 2.0 = 20.7$ MeV, $S_n = 18.7$ MeV). As a result, we observed a nearly doubled γ-ray emission rate in Fig. 10(c). With increasing E_x, the larger γ-ray emission rate and higher energy γ rays were observed until the excitation energy reached 27.2 MeV, which is the separation energy of the daughter nuclei ^{11}B ($S_{p'} = 11.2$ MeV) and ^{11}C ($S_{p'} = 8.7$ MeV). For $E_x > 27.2$ MeV, the ^{12}C state can decay via three-body decay to lighter nuclei. As far as hadronic decays are concerned, no γ rays with $E_\gamma > 11$ MeV were observed.[2]

[2]The study of electromagnetic decay of giant resonances in ^{12}C, emitting γ rays of $E_\gamma > 11$ MeV, will be reported elsewhere.

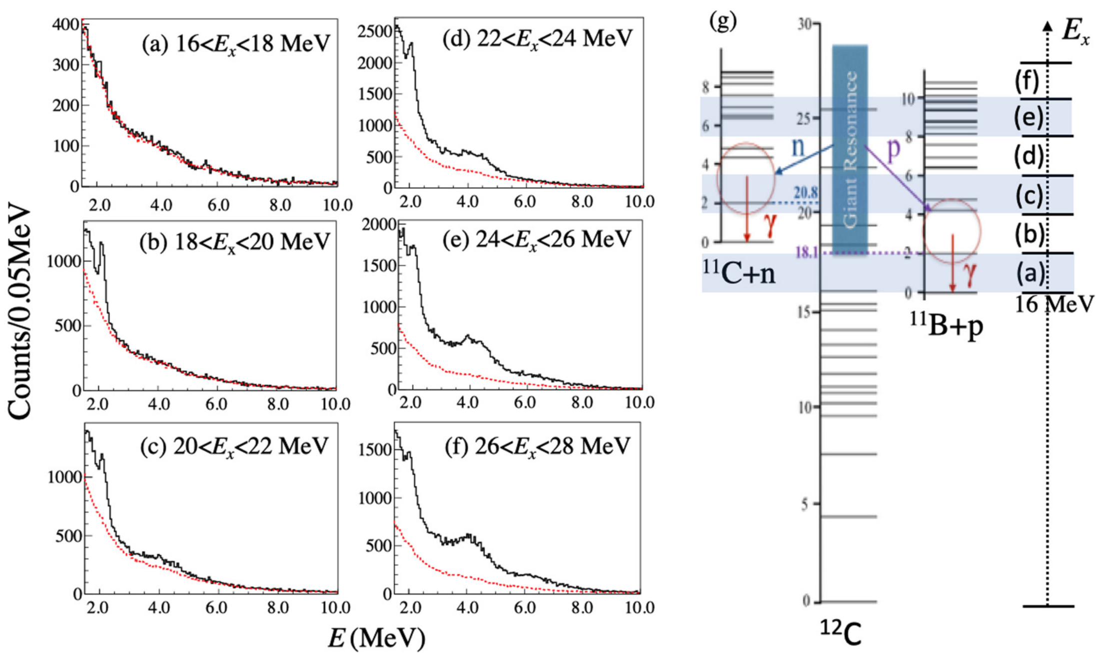

FIG. 10. (a)–(f) γ-ray energy spectrum (black solid line) and background energy spectrum (red dashed line) at various excitation energies in the giant resonance region of ^{12}C. (g) The decay scheme of ^{12}C*.

These features agree qualitatively with the theoretical predictions of Langanke *et al.* [11,12], which states that the γ rays from the giant resonances are emitted from the excited states of the daughter nuclei after hadronic decay. We will further analyze the γ-ray emissions quantitatively.

B. Extraction of the γ-ray emission probability $R_\gamma(E_x)$ from the fit to the γ-ray spectra

In order to obtain the γ-ray emission probability from the giant resonances of ^{12}C, we fit the data with γ-ray response functions generated for the excited states of the daughter nuclei, which can be defined as

$$P_i(E) = b_0\, P\big(E^i_\gamma; E\big) + \sum_{j=1} b_j\, P\big(E^i_\gamma - E^j_\gamma, E^j_\gamma; E\big), \qquad (4)$$

where $P_i(E)$ is the response function for the ith state of the daughter nuclei at energy E^i, b_0 is the probability for the ith state to decay directly to the ground state by emitting a γ ray of energy E^i_γ, and b_j is the probability for the ith state to decay to a lower energy state (E^j) by emitting a γ ray of energy $E^i_\gamma - E^j_\gamma$ and then decay to the ground state by emitting a γ ray of energy E^j_γ. For example, the first and the second excited states of ^{11}B decay directly to the ground state, emitting single γ rays with energies of 2.12 and 4.4 MeV, respectively, with $b_0 = 1.0$. Hence, their response functions are given as P(2.12 MeV;E) and P(4.4 MeV;E). The third excited state of ^{11}B decays to the ground state by emitting a 5.02-MeV γ ray with a probability of 0.85 (b_0) and to the 2.12-MeV state by emitting a 2.9-MeV γ ray (5.02−2.12 MeV) with a probability of 0.15 (b_1) followed by further decay to the ground state by the emission of a 2.12-MeV γ ray. The response function for this state is given as 0.85P(5.0 MeV;E)+0.15P(2.9, 2.12 MeV;E). Similarly, the response function for all of the other excited states of the daughter nuclei (^{11}B and ^{11}C) were generated by using the γ emission probabilities (b_0 and b_j) given in Ref. [10] and are listed in Table V. Once all of the response functions are generated, the efficiency (η_i) for the detection of γ rays emitted from the ith state of a daughter nucleus can be given as

$$\int_{E_{\rm th}}^{E_{\rm max}} P_i(E)dE = \eta_i. \qquad (5)$$

The total γ-ray emission probability in each E_x region of ^{12}C can be written as

$$R_\gamma(E_x) = \frac{\sigma_{p,p'\gamma}}{\sigma_{p,p'}} = \frac{N^0_\gamma}{N_{E_x}}, \qquad (6)$$

where N_{E_x} is the total number of excited states of ^{12}C in that E_x region and N^0_γ is the total number of γ rays emitted from these states. The contribution from the individual excited states (r_i) of the daughter nuclei (after particle decay) to the total γ-ray emission probability can be given as

$$r_i = \frac{N^0_i}{N_{E_x}} = \frac{N_i/\eta_i}{N_{E_x}}, \qquad (7)$$

TABLE V. Energy states, γ-ray energies and emission probabilities of the daughter nuclei, where we follow the notation used in Table of Isotope [10]. Energy of the deexciting transition is preceded by γ_a where a is energy of the level populated by that transition. The emission probabilities of one energy state (given in parentheses) are normalized to 1.0 [33].

Energy state (^{11}B)(MeV)	γ-ray energy (MeV)(prob.)	Energy state (^{11}C) (MeV)	γ-ray energy (MeV)(prob.)
2.12	$\gamma_0$2.12(1.0)	2.00	$\gamma_0$2.00(1.0)
4.44	$\gamma_0$4.44(1.0)	4.32	$\gamma_0$4.32(1.0)
5.02	$\gamma_0$5.02(0.85)	4.80	$\gamma_0$4.80(0.85)
	$\gamma_{2.12}$2.89(0.15)		$\gamma_{2.00}$2.80(0.15)
6.79	$\gamma_0$6.79(0.68)	6.34	$\gamma_0$6.34(0.67)
	$\gamma_{2.12}$4.66(0.28)		$\gamma_{2.00}$4.33(0.33)
	$\gamma_{5.02}$1.77(0.04)		
7.28	$\gamma_0$7.28(0.88)	6.90	$\gamma_0$6.90(0.92)
	$\gamma_{4.44}$2.84(0.05)		$\gamma_{4.32}$2.58(0.04)
	$\gamma_{5.02}$2.26(0.07)		$\gamma_{4.80}$2.10(0.04)
7.97	$\gamma_0$7.97(0.43)	7.49	$\gamma_0$7.49(0.36)
	$\gamma_{2.12}$5.85(0.49)		$\gamma_{2.00}$5.49(0.64)
	$\gamma_{7.28}$0.69(0.08)		
8.56	$\gamma_0$8.56(0.56)	8.10	$\gamma_0$8.10(0.74)
	$\gamma_{2.12}$6.43(0.30)		$\gamma_{2.00}$6.10(0.26)
	$\gamma_{4.44}$4.11(0.05)		
	$\gamma_{5.02}$3.54(0.09)		
8.92	$\gamma_0$8.92(0.95)	8.42	$\gamma_0$8.42(1.0)
	$\gamma_{4.44}$4.47(0.05)		
9.27	$\gamma_0$9.27(0.18)	9.20	$\gamma_0$9.20(0.74)
	$\gamma_{4.44}$4.83(0.70)		$\gamma_{6.47}$2.72(0.20)
	$\gamma_{6.74}$2.53(0.12)		$\gamma_{4.32}$4.88(0.13)

where N^0_i is the total number of γ rays emitted from the ith state of the daughter nucleus from the target and N_i is the number of events detected. The quantity r_i can also be interpreted as the probability for ^{12}C excited at E_x to decay to the ith state of the daughter nuclei and emit a γ ray. Furthermore, r_i can be decomposed as

$$r_i = C_{\rm GR}\, \tilde{r}_i + C_{\rm QF}\, r^i_{\rm QF}, \qquad (8)$$

where $C_{\rm GR}$ and $C_{\rm QF}$ are the fractions of giant resonances (GRs) and quasifree (QF) cross section in the total cross section obtained from Eq. (2), with

$$C_{\rm GR} + C_{\rm QF} = 1.0. \qquad (9)$$

$\tilde{r}_i$ is the probability of giant resonance decaying to the ith excited state of the daughter nuclei and $r^i_{\rm QF}$ is the probability of the daughter nuclei to be in the ith excited state after quasifree knockout. The estimation of γ-ray emission probability from quasifree process $r^i_{\rm QF}$ will be described in the next subsection, C. The measured γ-ray spectrum [$N_\gamma(E)$] in each E_x region can be expressed as

$$N_\gamma(E) = N_{E_x} \sum_i r_i\, P_i(E) + \alpha\, N_{bg}(E). \qquad (10)$$

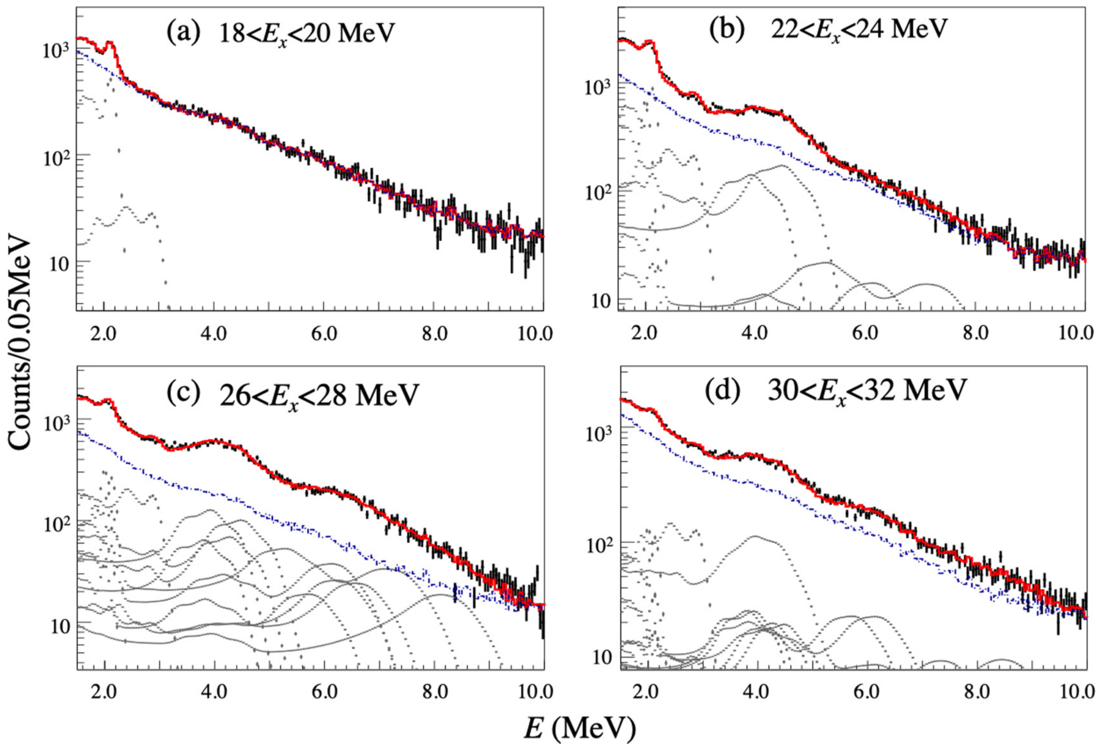

FIG. 11. The γ-ray spectrum (black data points), background spectrum (blue dash-dotted line), total fit (red solid line), and γ rays from the excited states of the daughter nuclei (grey dotted lines) are shown for various E_x regions.

Alternatively, this can be written as

$$N_\gamma(E) = N_{E_x}\left[C_{\rm GR}\sum_i \tilde{r}_i P_i(E) + C_{\rm QF}\sum_j r^j_{\rm QF} P_j(E)\right] + \alpha N_{bg}(E), \tag{11}$$

where $N_{bg}(E)$ and N_{E_x} are the background spectrum and the number of excitation events, respectively. The quantities r_i and the background normalization factor (α) were set as free parameters in the fit.

C. Estimation of γ-ray emission probability from quasifree processes

The probability ($r^j_{\rm QF}$) after quasifree nucleon knockout can be obtained as follows. A proton knockout from the $1p$ shell of ^{12}C leads to the $3/2^-$ ground state, the $1/2^-$ state at 2.1 MeV, and the $3/2^-$ state at 5.02 MeV in ^{11}B. The spectroscopic factors for $1p$ and $1s$ knockout from ^{12}C were experimentally determined from ^{12}C$(e, e'p)$ data and are listed in Refs. [43,44]. Using $1p$ spectroscopic factors, the probabilities for the daughter nucleus (^{11}B) to be in 2.1- and 5.02-MeV states were estimated to be ($r^{2.12}_{\rm QF}$ =) 4% and ($r^{5.02}_{\rm QF}$ =) 3%, respectively. It should be noted that for $E_x < 21$ MeV, only the 2.1-MeV state is energetically accessible with a probability of 4%, but as E_x exceeds 21 MeV, the 5.02-MeV state is also accessible. Similarly, a neutron knockout can also occur with equal probability and will lead to almost the same γ-ray response as that from a proton knockout. The only difference is that the threshold for neutron knockout is greater than that for proton knockout by 2.7 MeV.

For $E_x > 27.2$ MeV, $1s$ nucleon knockout can also occur. In this case, we used both $1s$ spectroscopic factor and statistical model calculations (described in the next section) to estimate the contribution to the γ-ray emission probability. It was less than 1% for $E_x = 27$–32 MeV and was therefore ignored.

Although 2.9-MeV γ rays are expected from the decay of several states (5.02, 7.28 MeV, etc.) and is included in their response functions, we found that an independent response function for 2.9 MeV must be added to Eq. (10) to obtain a good fit. Furthermore, during the fit, 6.74-MeV ($7/2^-$) and 6.79-MeV ($1/2^+$) states of ^{11}B and 6.48-MeV($7/2^-$) and 6.34-MeV($1/2^+$) states of ^{11}C were merged because these states lie close to each other and were assumed to have the same γ-ray response function. Some of the fitted spectra are shown in Fig. 11.

The total γ-ray emission probability in different E_x regions can be given as

$$R_\gamma(E_x) = \sum_i r_i = C_{\rm GR}\sum_i \tilde{r}_i + C_{\rm QF}\sum_j r^j_{\rm QF}. \tag{12}$$

This can be equivalently written as

$$R_\gamma(E_x) = \frac{(N_\gamma - N_{bg})/\bar{\eta}}{N_{E_x}}, \tag{13}$$

where N_γ, N_{bg}, and N_{E_x} are the number of γ-ray events, background events, and excitation events, respectively, and $\bar{\eta}$ is the weighted average efficiency in a particular E_x region and

TABLE VI. The probability (r_i) obtained from the fit and the total γ-ray emission probability $R_\gamma(E_x)$ with systematic errors. Numbers in the parentheses represent the error in the least significant digit.

Decay scheme	Energy state	^{12}C Excitation energy (E_x) (MeV)						
	(MeV) (J^π)	18–20	20–22	22–24	24–26	26–28	28–30	30–32
		r_i (%)						
^{11}B+p	2.12 ($1/2^-$)	7.6(2)	4.1(2)	9.2(2)	8.3(3)	5.9(3)	3.6(3)	2.8(4)
($S_p = 16.0$ MeV)	4.44 ($5/2^-$)		1.0(2)	3.0(2)	5.9(3)	5.9(3)	2.4(3)	1.2(4)
	5.02 ($3/2^-$)		1.2(2)	4.6(2)	5.7(3)	5.4(4)	2.9(5)	0.6(5)
	6.79 ($1/2^+$)			0.6(1)	4.3(4)	3.2(5)	3.2(6)	2.3(3)
	7.28 ($5/2^+$)				0.8(4)	1.7(3)	0.5(3)	0.4(3)
	7.97 ($3/2^+$)			0.9(1)	2.9(5)	4.5(5)		
	8.56 ($3/2^-$)				1.9(3)		2.9(3)	1.0(2)
	8.92 ($5/2^-$)					1.4(1)		
	9.27 ($5/2^+$)						2.8(7)	4.5(7)
^{11}C+n	2.00 ($1/2^-$)		2.4(1)	5.9(1)	6.5(2)	5.9(3)	3.6(3)	2.8(4)
($S_n = 18.7$ MeV)	4.32 ($5/2^-$)				1.0(1)	3.0(2)	2.4(3)	1.2(4)
	4.80 ($3/2^-$)				3.2(2)	3.6(3)	2.2(4)	0.6(5)
	6.34 ($1/2^+$)					1.6(2)	1.1(2)	2.3(4)
	6.90 ($5/2^+$)					1.7(3)	0.5(3)	0.4(3)
	7.49 ($3/2^+$)							
	8.10 ($3/2^-$)						1.5(1)	1.0(2)
	8.42 ($5/2^-$)							
	9.20 ($5/2^+$)						0.3(1)	0.5(1)
QF	2.12 ($1/2^-$)	0.3(1)	0.9(2)	0.8(2)	1.4(3)	1.8(3)	2.2(3)	2.9(5)
	5.02 ($3/2^-$)		0.3(1)	0.3(1)	1.0(2)	1.3(2)	1.7(2)	2.2(5)
	2.9	0.8(2)	1.2(2)	4.2(2)	6.3(3)	7.5(4)	6.1(4)	6.0(4)
$R_\gamma(E_x)$ (%)		8.4 ± 0.5	11.1 ± 0.6	28.6 ± 1.6	48.3 ± 3.5	53.3 ± 3.9	39.3 ± 2.9	33.3 ± 2.5

$\bar{\eta}$ is given as

$$\begin{aligned}\bar{\eta} &= \frac{1}{\Sigma r_i}\sum_i r_i\eta_i \\ &= \frac{1}{C_{\mathrm{GR}}\sum_i \tilde{r}_i + C_{\mathrm{QF}}\sum_j r^j_{\mathrm{QF}}} \\ &\quad\times\left(C_{\mathrm{GR}}\sum_i \tilde{r}_i\eta_i + C_{\mathrm{QF}}\sum_j r^j_{\mathrm{QF}}\eta_j\right).\end{aligned} \tag{14}$$

The total γ-ray emission probability and the probability (r_i) obtained from the fit are shown in Table VI for all E_x regions.

VI. RESULTS OF γ-RAY EMISSION PROBABILITY $R_\gamma(E_x)$ AND DISCUSSION

A. γ-ray emission probability

The γ-ray emission probability $R_\gamma(E_x)$ as a function of excitation energy (E_x) is shown in Fig. 12 along with both statistical and systematic errors. The systematic uncertainties include the errors in the determination of excitation events (2–3%), γ-ray background subtraction (1–3%), and detection efficiency (5–7%). The errors due to statistical uncertainty were 0.7–3%. The γ-ray emission probability increases with the increasing excitation energy, starting from zero at $E_x =$ 16 MeV and reaches a maximum value of $53.3 \pm 0.4 \pm 3.9\%$ at $E_x = 27$ MeV, where the first and second uncertainties are statistical and systematic, respectively. For $E_x > 27$ MeV, the emission probability gradually decreases with the increasing excitation energy. This feature is discussed later in detail. The most dominant contributions to the emission probability come from the 2.1- and 2.0-MeV states (first excited states of ^{11}B and ^{11}C, respectively). For $E_x > 26$ MeV, the contributions of

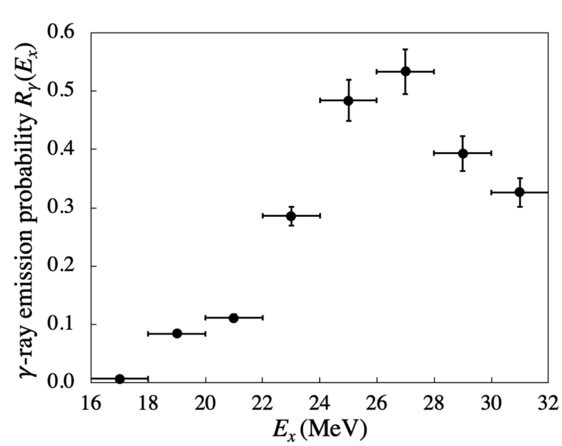

FIG. 12. Total γ-ray emission probability $R_\gamma(E_x)$ as a function of E_x. The error bars include both statistical and systematic uncertainties.

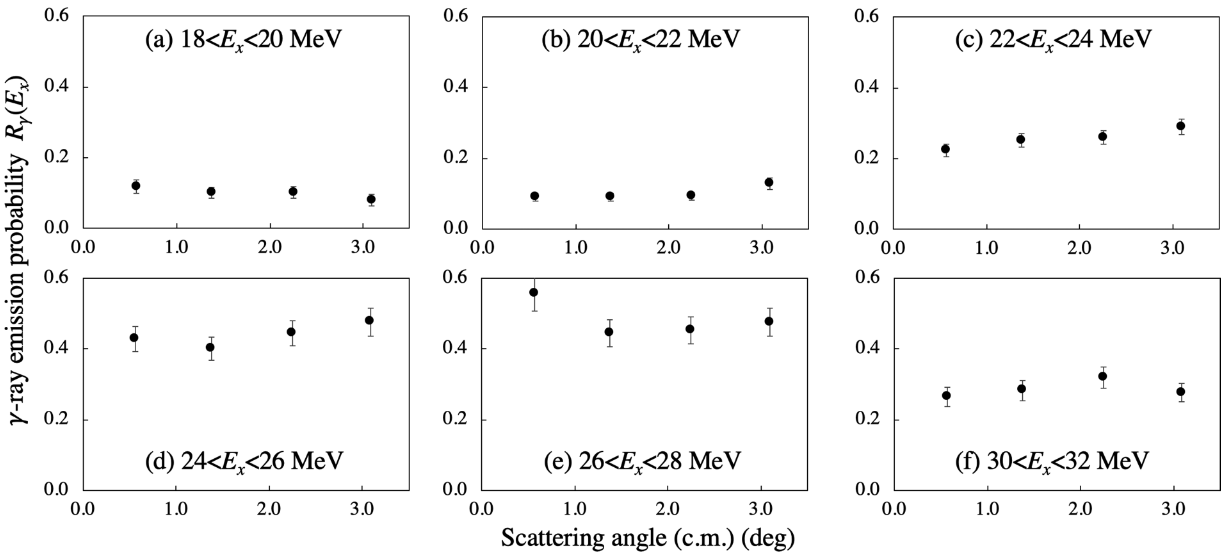

FIG. 13. The γ-ray emission probability as a function of scattering angle at various excitation energies in the giant resonance region of ^{12}C.

8–9-MeV states of the daughter nuclei also become significant (Table VI).

The γ-ray emission probability was also measured as a function of scattering angle for different E_x regions and no strong angular dependence was observed (Fig. 13).

B. Comparison with decay model prediction

A statistical model calculation based on the Hauser-Feshbach formalism [45,46] was used to predict the γ-ray emission probability from the giant resonances of ^{12}C and is described as follows. The transmission coefficient from an excited nucleus (E_x) to the ith energy state of a daughter nucleus $A(E_A^i, J_A^i, \pi_A^i)$ by the emission of particle a is given by the summation over all quantum mechanically allowed partial waves,

$$T[E_x \to a + (A, i)] = \sum_{S=|J_A^i - s_a|}^{J_A^i + s_a} \sum_{L=|J_x - S|}^{J_x + S} T_L^a(\epsilon_a), \tag{15}$$

where $T_L^a(\epsilon_a)$ is the individual transmission coefficient of the particle a with kinetic energy ϵ_a given by $E_x - E_A^i -$separation energy, spin s_a, and orbital angular momentum L. The summation over L is restricted by the parity conservation rule $\pi_x = \pi_a \pi_A^i (-1)^L$. These individual transmission coefficients were obtained by solving the Schrödinger equation with the optical potential for the particle nucleus interaction [47,48]. We employed global optical potential parameters given in Refs. [49–52] for the calculations.

The decay of an excited nucleus can proceed via different channels $a = p,\ n,\ d,\ t$, and α. Then, the probability for an excited nucleus (E_x) to decay to the ith state of the daughter nuclei can be given as

$$\tilde{c}_i = \frac{\beta_a\, T[E_x \to a + (A, i)]}{\sum_{a,i} \beta_a\, T[E_x \to a + (A, i)]}, \tag{16}$$

where β_a is the isospin Clebsch Gordan coefficient [53,54]. We used the spin-parity information of Table II for the resonance states in different E_x regions and calculated the γ-ray spectrum $N_\gamma^{\rm calc}(E)$ as

$$N_\gamma^{\rm calc}(E) = N_{E_x}\left[C_{\rm GR}\sum_i \tilde{c}_i\, P_i(E) + C_{\rm QF}\sum_j r_{\rm QF}^j\, P_j(E)\right] + \alpha\, N_{bg}(E). \tag{17}$$

It should be noted that $\tilde{r}_i$ in Eq. (11) is replaced by $\tilde{c}_i$ in Eq. (17). Accordingly, the calculated γ-ray emission probability $R_\gamma^{\rm calc}(E_x)$ can be determined as

$$R_\gamma^{\rm calc}(E_x) = C_{\rm GR}\sum_i \tilde{c}_i + C_{\rm QF}\sum_j r_{\rm QF}^j. \tag{18}$$

This probability is also shown in Fig. 14 as a red (solid) line. The γ-ray emission probability from the quasifree process is also shown (blue dash-dotted line).

The main contribution to the total γ-ray emission probability [$R_\gamma^{\rm calc}(E_x)$] comes from the decay of giant resonances. For $E_x = 16$–27 MeV, $R_\gamma^{\rm calc}(E_x)$ increases because $C_{\rm GR}$ dominates in this energy region and the number of accessible states of the daughter nuclei also increases. For $E_x > 27$ MeV, $C_{\rm GR}$ begins to decrease and so does the γ-ray emission probability, while the contribution of $C_{\rm QF}$ becomes nearly equal to $C_{\rm GR}$. The red band in Fig. 14 shows the uncertainty in the calculation due to the uncertainty in $C_{\rm QF}$ ($\mu = 1.27 \pm 0.25$).

The statistical model calculations predicted a higher decay probability to the excited states by 30–40% as compared to the measured values in the energy region $E_x = 20$–24 MeV. The same feature was observed when we compared calculations with the measurement of ^{12}C(γ, total) and ^{12}C(γ, n_0) cross sections [28].

For $E_x > 27.2$ MeV, the three-body decay threshold is reached, and the decay involving two-nucleon emission ($p + p + {}^{10}$Be) also starts. Although the decay via three-body process was significant (≈6%), it gave negligible contribution (<1%) to the γ-ray emission probability.

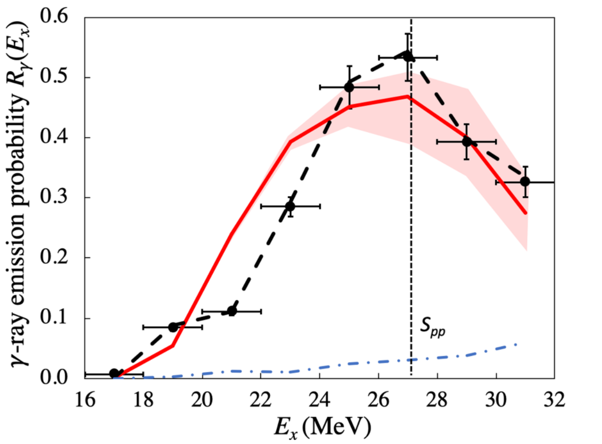

FIG. 14. Comparison between the measured γ-ray emission probability (data points) and the statistical model prediction (red solid line). The black dashed line shows the γ-ray emission probability obtained from the fit [Eq. (12)]. The red band shows the uncertainty in calculation due to the error in C_{QF}. The γ-ray emission probability from quasifree process (blue dash-dotted line) is also shown. The quantity S_{pp} represents the two proton emission threshold (27.2 MeV) for ^{12}C.

VII. CONCLUSION

We measured the double differential cross section ($d^2\sigma/dE_x d\Omega$) for the ^{12}C(p, p') inelastic reaction at 392 MeV and 0° for the energy range $E_x = 7$–32 MeV. Furthermore, the cross section was decomposed into spin-flip ($\Delta S = 1$) and non-spin-flip ($\Delta S = 0$) components by using polarization transfer (PT) observables measured previously at the same beam energy [21]. The spin-flip cross section was observed to be dominated by isovector resonances and the non-spin-flip cross section was dominated by 1^- resonances and agreed well with recent calculations of Coulomb excitations [27].

For the measurements of γ rays from the giant resonances, the absolute values of the γ-ray emission probability $R_\gamma(E_x)$ and the response functions were verified by using *in situ* γ rays (15.1 and 6.9 MeV) with an accuracy of $\pm5\%$ during the experiment. This calibration procedure made it possible to measure $R_\gamma(E_x)$ reliably as a function of the excitation energy of ^{12}C in the energy range $E_x = 16$–32 MeV. We found that the measured value of $R_\gamma(E_x)$ starts from zero at $E_x = 16$ MeV (the threshold of $p + {}^{11}$B decay) and increases to $53.3 \pm 0.4 \pm 3.9\%$ at $E_x = 27$ MeV and begins to decrease with further increase in E_x.

We compared the measurements of γ-ray emission probability with a statistical model calculation to understand our measured values. For $E_x = 16$–27 MeV, the γ-ray emission probability increases with excitation energy because this energy region is dominated by giant resonances and the number of accessible states of the daughter nuclei also increases. For $E_x > 27$ MeV, the dominance of giant resonances ceases and we observe the corresponding decrease in the γ-ray emission probability. In this energy region, the contribution from quasifree process to the total cross section becomes nearly equal to that of giant resonances, but still its total contribution to the γ-ray emission probability is at most 5% as shown in Fig. 14 (blue line). We also found that the contribution of three-body decay process to the γ-ray emission probability was negligible. Quantitatively, we observed a 30–40% lower γ-ray emission probability in the energy region $E_x = 20$–24 MeV than that predicted by the statistical model calculation.

The γ-ray emission probability was also measured as a function of scattering angle, but no strong angular dependence was observed.

The present results are very important for understanding the γ-ray emission probability of the giant resonances of a typical light nucleus (^{12}C) and for the neutrino detection in liquid scintillator detectors through neutral-current interactions. A similar analysis of the ^{16}O(p, p') reaction is ongoing and will be presented elsewhere. An experiment with a germanium detector such as that of the CAGRA spectrometer at RCNP [55] will significantly improve the current understanding of the γ-ray emission and decay of giant resonances by separating γ rays emitted from the daughter nuclei after proton and neutron decays.

ACKNOWLEDGMENTS

We gratefully acknowledge the outstanding efforts of the RCNP cyclotron staff for providing a clean and stable beam for our experiment. We would like to thank Prof. H. Toki, the former Director of RCNP, for encouraging us at the early stage of this experiment. We also thank Prof. M. N. Harakeh, Prof. Y. Suda, Prof. H. Chiba, and Prof. H. Sagawa for valuable discussions. This work was supported by JSPS Grant-in-Aid for Scientific Research on Innovative Areas (Research in a proposed research area) Grant No. 26104006.

[1] E. Anders and N. Grevesse, Geochim. Cosmochim. Acta **53**, 197 (1988).
[2] F. Reines and C. L. Cowan, Phys. Rev. **92**, 830 (1953); Nature (London) **178**, 446 (1956).
[3] A. Suzuki, Nucl. Phys. B, Proc. Suppl. **77**, 171 (1999); K. Tolich *et al.* (KamLAND Collaboration), *ibid.* **221**, 355 (2011).
[4] B. Bodmann *et al.*, Phys. Lett. B **267**, 321 (1991).
[5] B. Armbruster *et al.*, Phys. Lett. B **423**, 15 (1998).
[6] C. Athanassopoulos *et al.* (LSND Collaboration), Phys. Rev. Lett. **75**, 2650 (1995).
[7] H. A. Bethe, Rev. Mod. Phys. **62**, 801 (1990).
[8] K. Hirata *et al.* (Kamiokande Collaboration), Phys. Rev. Lett. **58**, 1490 (1987).
[9] J. S. O'Connell, T. W. Donnelly, and J. D. Walecka, Phys. Rev. C **6**, 719 (1972); T. W. Donnelly and R. Peccei, Phys. Rep. **50**, 1 (1979).

[10] *Table of Isotopes*, 1999 Update with CD-ROM, 8th ed., edited by R. B. Firestone, C. M. Baglin, and S. Y. F. Chu (Wiley, New York, 1999).
[11] K. Langanke, P. Vogel, and E. Kolbe, Phys. Rev. Lett. **76**, 2629 (1996).
[12] E. Kolbe, K. Langanke, S. Krewald, and F. K. Thielemann, Nucl. Phys. A **540**, 599 (1992).
[13] Y-Z. Qian and G. M. Fuller, Phys. Rev. D **49**, 1762 (1994).
[14] R. Buras, H.-T. Janka, M. Keil, G. Raffelt, and M. Rampp, Astrophys. J. **587**, 320 (2003).
[15] P. von Neumann-Cosel and A. Tamii, Eur. Phys. J. A **55**, 110 (2019).
[16] A. Tamii *et al.*, IEEE Trans. Nucl. Sci. **43**, 2488 (1996).
[17] M. Fujiwara *et al.*, Nucl. Instrum. Methods Phys. Res., Sect. A **422**, 484 (1999).
[18] A. Tamii *et al.*, Nucl. Instrum. Methods Phys. Res., Sect. A **605**, 326 (2009).
[19] G. J. F. Legge and I. F. Bubb, Nucl. Phys. **26**, 616 (1961).
[20] J. K. Bair, C. M. Jones, and H. B. Willard, Nucl. Phys. **53**, 209 (1964).
[21] A. Tamii *et al.*, Phys. Lett. B **459**, 61 (1999); A. Tamii, doctoral dissertation, Kyoto University, 1999.
[22] T. Kawabata *et al.*, Phys. Rev. C **65**, 064316 (2002); T. Kawabata, doctoral dissertation, Kyoto University, 2002.
[23] M. Dozono *et al.*, J. Phys. Soc. Jpn. **77**, 014201 (2008).
[24] B. D. Anderson, L. A. C. Garcia, D. J. Millener, D. M. Manley, A. R. Baldwin, A. Fazely, R. Madey, N. Tamimi, J. W. Watson, and C. C. Foster, Phys. Rev. C **54**, 237 (1996).
[25] W. G. Love and M. A. Franey, Phys. Rev. C **24**, 1073 (1981); **27**, 438(E) (1983); **31**, 488 (1985).
[26] F. Petrovich and W. G. Love, Nucl. Phys. A **354**, 499 (1981).
[27] C. A. Bertulani and A. M. Nathan, Nucl. Phys. A **554**, 158 (1993).
[28] E. G. Fuller, Phys. Rep. **127**, 185 (1985).
[29] T. Ishikawa *et al.*, Nucl. Phys. A **687**, 58 (2001).
[30] B. N. Johnson *et al.*, Phys. Rev. C **51**, 1726 (1995).
[31] M. Itoh *et al.*, Nucl. Phys. A **738**, 268 (2004).
[32] A. Kiss, C. M. Böricke, M. Rogge, P. Turek, and S. Wiktor, J. Phys. G: Nucl. Phys. **13**, 1067 (1987).
[33] J. H. Kelley, J. E. Purcell, and C. G. Sheu, Nucl. Phys. A **968**, 71 (2017).
[34] A. Erell, J. Alster, J. Lichtenstadt, M. A. Moinester, J. D. Bowman, M. D. Cooper, F. Irom, H. S. Matis, E. Piasetzky, and U. Sennhauser, Phys. Rev. C **34**, 1822 (1986).
[35] J. Raynal, program code "DWBA07" NEA-1209/08.
[36] T. Suzuki, R. Fujimoto, and T. Otsuka, Phys. Rev. C **67**, 044302 (2003).
[37] J. B. Flanz, R. S. Hicks, R. A. Lindgren, G. A. Peterson, A. Hotta, B. Parker, and R. C. York, Phys. Rev. Lett. **41**, 1642 (1978).
[38] K. W. Jones *et al.*, Phys. Rev. C **50**, 1982 (1994).
[39] T. Yoshida, T. Suzuki, S. Chiba, T. Kajino, H. Yokomakura, K. Kimura, A. Takamura, and D. H. Hartmann, Astrophys. J. **686**, 448 (2008).
[40] J. R. Comfort, G. L. Moake, C. C. Foster, P. Schwandt, and W. G. Love, Phys. Rev. C **26**, 1800 (1982).
[41] S. Cohen and D. Kurath, Nucl. Phys. **73**, 1 (1965).
[42] Geant4 Collaboration, Geant4 Physics Reference Manual for Geant4 version 9.6.0 (2012). https://geant4.web.cern.ch/support/download_archive?page=5.
[43] L. Lapikas, G. van der Steenhoven, L. Frankfurt, M. Strikman, and M. Zhalov, Phys. Rev. C **61**, 064325 (2000).
[44] G. Van Der Steenhoven, H. P. Blok, E. Jans, M. De Jong, L. Lapikás, E. N. M. Quint, and P. K. A. De Witt Hubert, Nucl. Phys. A **480**, 547 (1988).
[45] W. Hauser and H. Feshbach, Phys. Rev. **87**, 366 (1952).
[46] T. Rauscher, F. K. Thielemann, and K. L. Kratz, Phys. Rev. C **56**, 1613 (1997).
[47] F. Puhlhofer, Nucl. Phys. A **280**, 267 (1977).
[48] K. H. N. Murthy, S. K. Gupta, and A. Chatterjee, Z. Phys. A **305**, 73 (1982).
[49] J. Rapaport *et al.*, Nucl. Phys. A **330**, 15 (1979).
[50] F. D. Becchetti and G. W. Greenlees, Phys. Rev. **182**, 1190 (1969).
[51] G. R. Satchler, Nucl. Phys. **70**, 177 (1965).
[52] G. Perrin, Nguyen Van Sen, J. Arvieux, R. Darves-Blanc, J. L. Durand, A. Fiore, J. C. Gondrand, F. Merchez, and C. Perrin, Nucl. Phys. A **282**, 221 (1977).
[53] S. M. Grimes, J. D. Anderson, A. K. Kerman, and C. Wong, Phys. Rev. C **5**, 85 (1972).
[54] M. N. Harakeh, D. H. Dowell, G. Feldman, E. F. Garman, R. Loveman, J. L. Osborne, and K. A. Snover, Phys. Lett. B **176**, 297 (1986).
[55] C. Sullivan *et al.*, Phys. Rev. C **98**, 015804 (2018).